a beta pdf multiplied by a general function is performed with a numerical integration employing the methodology described in [44]. The integrals must cover the range $Z(0,1)$, but there are possible singularities at Z=0 and Z=1 (improper integrals) when the beta pdf is employed. The method consist on dividing the integral of the product $\phi(Z)P(Z)$ in three parts:

$$\int_0^1 \phi(Z)P(Z)dZ = \int_0^\epsilon \phi(Z)P(Z)dZ + \int_\epsilon^{1-\epsilon} \phi(Z)P(Z)dZ + \int_{1-\epsilon}^1 \phi(Z)P(Z)dZ \quad (4.55)$$

where ϵ is a small value set to 10^{-4}. This beta pdf can be written as follows:

$$P(Z) = Z^{\alpha-1}(1-Z)^{\beta-1}G \qquad \text{with} \qquad G = \frac{\Gamma(\alpha+\beta)}{\Gamma(\alpha)\Gamma(\beta)} \quad (4.56)$$

Introducing Eq. 4.56 into Eq. 4.55 and after integrating the first and the last term of the r.h.s:

$$\int_0^1 \phi(Z)P(Z)dZ \approx \phi(0)\frac{\epsilon^\alpha G}{\alpha} + G\int_\epsilon^{1-\epsilon} \phi(Z)Z^{\alpha-1}(1-Z)^{\beta-1}dZ + \phi(1)\frac{\epsilon^\beta G}{\beta} \quad (4.57)$$

where the integral (second term on the r.h.s.) is evaluated using the *QAGS adaptive integration with singularities* function of the GSL (GNU Scientific Library) [45].

4.7.1 Verification of numerical solutions

Numerical results have been submitted to the verification procedure described in section 1.4.5. The h-refinement study is performed with five levels of refinement ($n = 1, 2, 4, 8$ and 16). For example, for the finest discretization $n = 16$, 197.120 CVs are employed. Estimations are given for a zone limited by the following equation of a straight line:

$$r = r_p + \frac{15d - r_p}{100d}z \quad (4.58)$$

which is in fact the space region that encloses the flame. In this equation, d=7.2 mm is the main jet inner diameter and r_p=9.1 mm is the piloted annulus outer radius.

The results obtained considering steady flamelet modelling, assuming unity Lewis number for all species and adiabatic flame conditions, are shown in Table 4.1. Otherwise, verification results for the EDC model using the four-step mechanism and considering radiation heat transfer and differential diffusion, are exposed in Table 4.2. Verification results are presented for the refinement levels $n = 4, 8$ and 16. The maximum temperature at the centerline and the flame height are also shown exhibiting an asymptotic behaviour.

Steady flamelet modelling with Unity-Lewis ($Le_i = 1$) and No-Radiation						
grid	$T_{max,C}$	Hf	GCI^* [%]			
n	$[K]$	$[cm]$	$\widetilde{v^*}_r = \widetilde{v}_r/v_{in}$	$\widetilde{v^*}_z = \widetilde{v}_z/v_{in}$	$\widetilde{Z}$	$\widetilde{Z''^2}$
4	2044.83	33.64	0.042	0.44	0.29	0.014
8	2043.49	33.83	0.010	0.20	0.12	0.006
16	2042.75	33.73	0.006	0.11	0.06	0.002

Table 4.1: Verification of numerical solutions for SF. (n: grid parameter; $T_{max,C}$: maximum temperature at the symmetry axis; Hf: flame height; GCI: Grid Convergence Index). v_{in}=49.6 m/s and T_{in}=294 K.

Eddy Dissipation Concept (EDC) model with the four-step mechanism (4S)					
grid	$T_{max,C}$	Hf	GCI^* [%]		
n	$[K]$	$[cm]$	$\widetilde{v^*}_r = \widetilde{v}_r/v_{in}$	$\widetilde{v^*}_z = \widetilde{v}_z/v_{in}$	$\widetilde{T^*} = \widetilde{T}/T_{in}$
4	2044.83	33.64	0.04	0.40	4.80
8	2043.49	33.83	0.02	0.26	3.00
16	2042.75	33.73	0.01	0.16	1.60

Table 4.2: Verification of numerical solutions for EDC. See caption of Table 4.1.

The number of Richardson nodes observed is larger than 75% for all the independent variables and the observed order of accuracy p correspond to its theoretical value since the upwind scheme is used for the convective terms. The grid convergence index (GCI) gives the error band where the grid independent solution is expected to be contained, say the uncertainty due to discretization. The GCI values divide by a factor of approximately two from mesh to mesh. This behaviour is in concordance to the theoretical response.

Analysing GCI values, the numerical solution obtained with the fourth level of refinement $n = 8$ can be considered to be accurate enough. The velocity uncertainties of steady flamelet simulations have a value of $\pm 0.01\%$ for the radial component and a value of $\pm 0.2\%$ for the axial component. The verification results for the mixture fraction variable exhibit also a proper behaviour. Verification results for the EDC model show similar trends. For this model, the dimensional value of the temperature uncertainty corresponding to the level of refinement $n = 8$ is approximately ± 8.8 K which is considered to be accurate enough.

As a result of this verification study, all the simulations hereinafter presented are performed with the fourth level of refinement ($n = 8$, i.e. 51456 CVs).

4.8 Results and discussion

The piloted non-premixed methane/air turbulent flame is analysed comparing the verified numerical results with the experimental data available in the literature [8]. Centerline profiles for temperature and mass fractions of some species (viz. CO_2, H_2O, H_2, OH, CO and NO) are provided. Moreover, radial profiles of the same variables are given for the flame heights z/d=3, 7.5, 15, 30, 45 and 60. Results discussion is supported by figures 4.5-4.16.

Numerical results are presented considering radiation heat transfer and the differential diffusion effect. However, when radiation is not considered (adiabatic flame) it is indicated in the figure legends with the terminology **Adiab** and when differential diffusion is not taken into account (unity-lewis number), it is indicated by $\boldsymbol{Le = 1}$.

4.8.1 Eddy Dissipation Concept model simulations

The main goal of the present thesis is the analysis of the laminar flamelet concept for both laminar and turbulent flame simulations. Results presented in this section considering the Eddy Dissipation Concept model are used as an illustrative result of the performance of a simpler and widely used model in commercial codes extensively applied in industry.

Figure 4.5 shows centerline profiles of temperature and CO_2 mass fraction comparing both chemical mechanisms (SS and 4S) as well as experimental data [8]. Figures 4.6 and 4.7 present the radial profiles for the same variables. Numerical solutions assuming adiabatic flame conditions and unity-Lewis numbers are shown in order to highlight the influence of radiation heat transfer and differential diffusion effects.

It is important to keep in mind that for both reduced mechanisms (SS and 4S) there are several model constants that are susceptible to be "tuned" depending on the particular flame simulated, specially for the irreversible single-step mechanism. In addition to the kinetic constants to evaluate the Arrhenius term, taken from [35] for SS and [36] for 4S, there are the specific modelling constants (C_{EDC} and B) of the EDC model.

All numerical simulations that use the single step mechanism (SS) clearly overpredict the temperature along the centerline profile, and all the temperature radial profiles for each height. Figure 4.5 shows a proper prediction of temperature increase, but the maximum peak temperature is approximately 7 cm higher. The peak temperature profile is not a sharp peak, but a wide zone. A similar behaviour is observed for the CO_2 mass fraction. The production of CO_2 is much larger than the production obtained experimentally.

Otherwise, numerical results obtained taking into account the four-step mechanism (4S) exhibit a significant improvement compared to SS of both temperature and CO_2 mass fraction. The centerline profile of temperature shows a proper description of

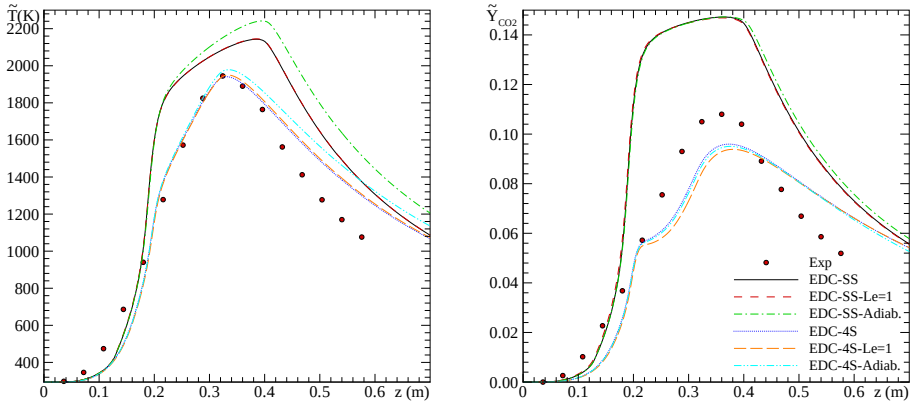

Figure 4.5: Centerline profiles for the turbulent piloted methane/air jet flame (Flame D). Eddy dissipation concept (EDC) simulations: (a) Centerline temperature; (b) Centerline CO_2 mass fraction. Experimental results in [8].

the temperature behaviour at jet entrance, a good description of the temperature gradient found and a proper description of the temperature peak and its height. At the post-flame region the temperature is slightly over-predicted. This behaviour can also be observed in the radial profiles. On the other hand, the centerline profile of CO_2 shows a poor prediction of the experimental data, describing an advanced and too large production peak and a large over-prediction at the post-flame region. Otherwise, the radial profiles show a proper behaviour for low heights (z/d=3, 7.5, 15) and an under-prediction of the profile at z/d=30 and 45.

Radiation heat transfer influence has deep impact when the single-step mechanism (SS) is used. The radiation begins to have a strong impact at a height of approximately 21 cm, which is still in the inner-flame region. The maximum temperature difference when radiation heat transfer is considered or neglected is of more than 140 K. Otherwise, when the four-step mechanism (4S) is used, the influence of radiation is distinguished after the flame-front (post-flame region). In this case, the influence of radiation is weaker than for the SS mechanism, only producing a maximum temperature difference of approximately 100 K between adiabatic flame consideration and the radiative one. Radiation has a poor impact on the prediction of CO_2 mass fraction for both mechanisms.

Differential diffusion exhibit a very weak effect for both mechanisms. For high Reynolds number zones, the molecular mass diffusion term, $\nabla \cdot \overline{\vec{j}_i}$, present in Eq.

4.13 and modelled in section 4.4.4, has a very little impact compared to the scalar turbulent flux term, $\nabla \cdot (\overline{\rho}\widetilde{\vec{v}''Y_i''})$, also present in Eq. 4.13 and modelled in section 4.4.3. Therefore, the consideration of unity-Lewis number or fixed Lewis number for each species is not sensible for flames where weak laminarized or re-laminarized zones are present.

In summary, the SS mechanism exhibits a clear over-prediction of the thermal field and the CO_2 mass fraction. The 4S mechanism properly describe the main flame trends. Even though, the simplified chemistry involved in the mentioned mechanisms make these modelizations not adequate to predict important aspects of the flame such as pollutant formation. These reduced mechanisms allow to predict the general trends of the flame, say temperature and major species, with a reasonable computational effort and a slightly simple mathematical formulation.

4.8.2 Flamelet modelling simulations

Flamelet simulations are here presented in order to show the limitations and capabilities of each approach considering or neglecting the transient term of the flamelet equations and also taking into account the two phenomenological aspects indicated above: radiation and differential diffusion. Regarding the know-how achieved in the previous chapter of the present thesis, the steady flamelets are considered without differential diffusion and with adiabatic flame conditions (no radiation). Otherwise, unsteady flamelets are used to include differential diffusion and radiation, and also to properly predict the pollutant formation. Radiation and CO and NO_x production/destruction are slow phenomena that require the transient term of the flamelet equations. Also, this term allows to balance the *super-equilibrium* phenomena [46, 47] that appear when steady flamelets are used. Unsteady flamelets are also presented considering adiabatic flame conditions (Adiab) and without differential diffusion ($Le = 1$).

Figures 4.8a and 4.9b show the axial temperature behaviour along the centerline for both the axial coordinate and also conditioned to the Favre-averaged mixture fraction $\widetilde{Z}$. Radial temperature profiles at z/d=3, 7.5, 15, 30, 45 and 60 are shown in figures 4.10 and 4.11. Referring to the species mass fractions, figures 4.8 and 4.9 show the axial profiles of H_2O, CO_2, H_2, OH, CO and NO. Radial profiles for the mass fraction of CO_2, H_2, OH, CO and NO are shown in figures 4.10-4.15.

Eddy dissipation concept model using the four-step mechanism (4S) has also been included in the figures to show the performance of this model compared to flamelet modelling simulations. This comparison should be carefully studied since flamelet models are used with a finite rate chemistry and the mechanism employed with EDC is strongly reduced.

Steady flamelet (SF) approach results for the thermal field agree with the experimental data in the inner flame zone where radiation is not important. Otherwise,

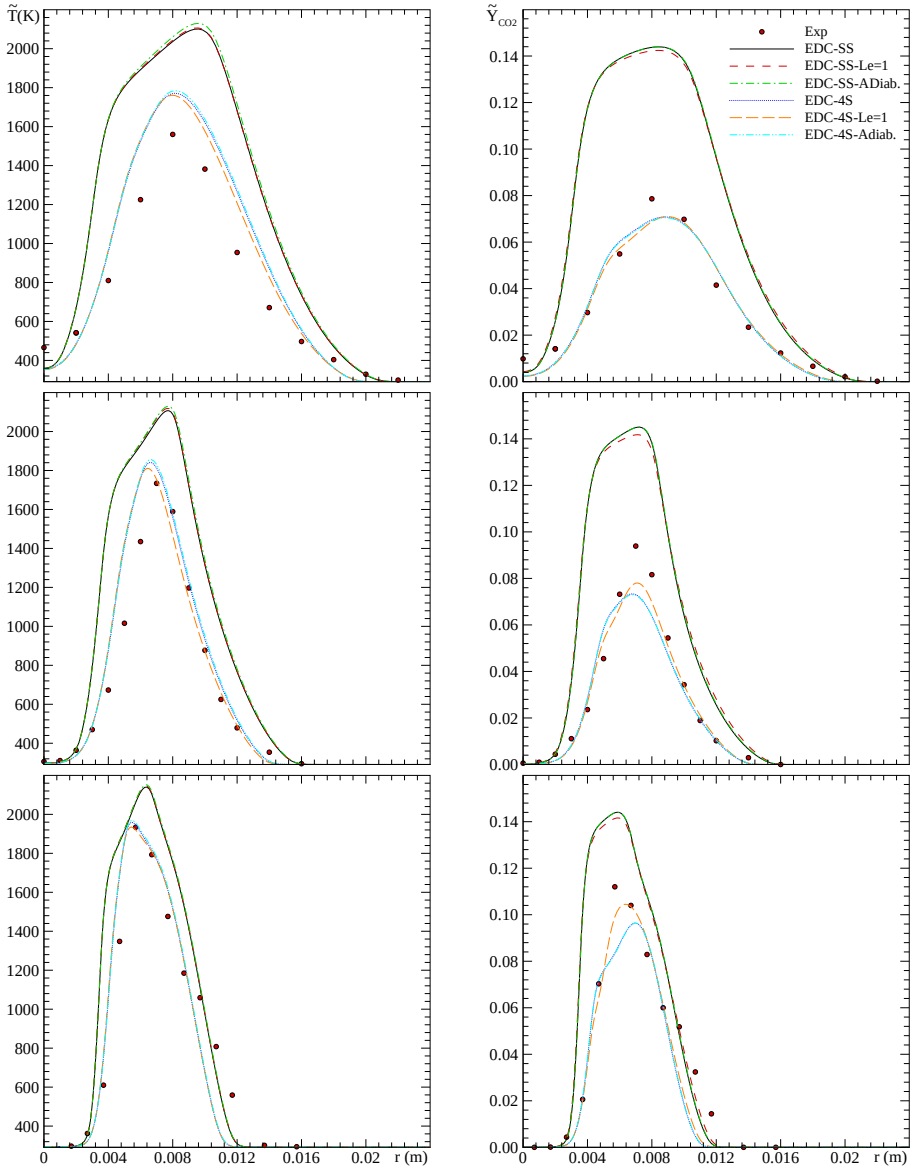

Figure 4.6: Radial profiles for the turbulent piloted methane/air jet flame (Flame D). Eddy dissipation concept (EDC) simulations: z/d=3, 7.5 and 15 (left: Temperature; right: CO_2 mass fraction). Experimental results in [8].

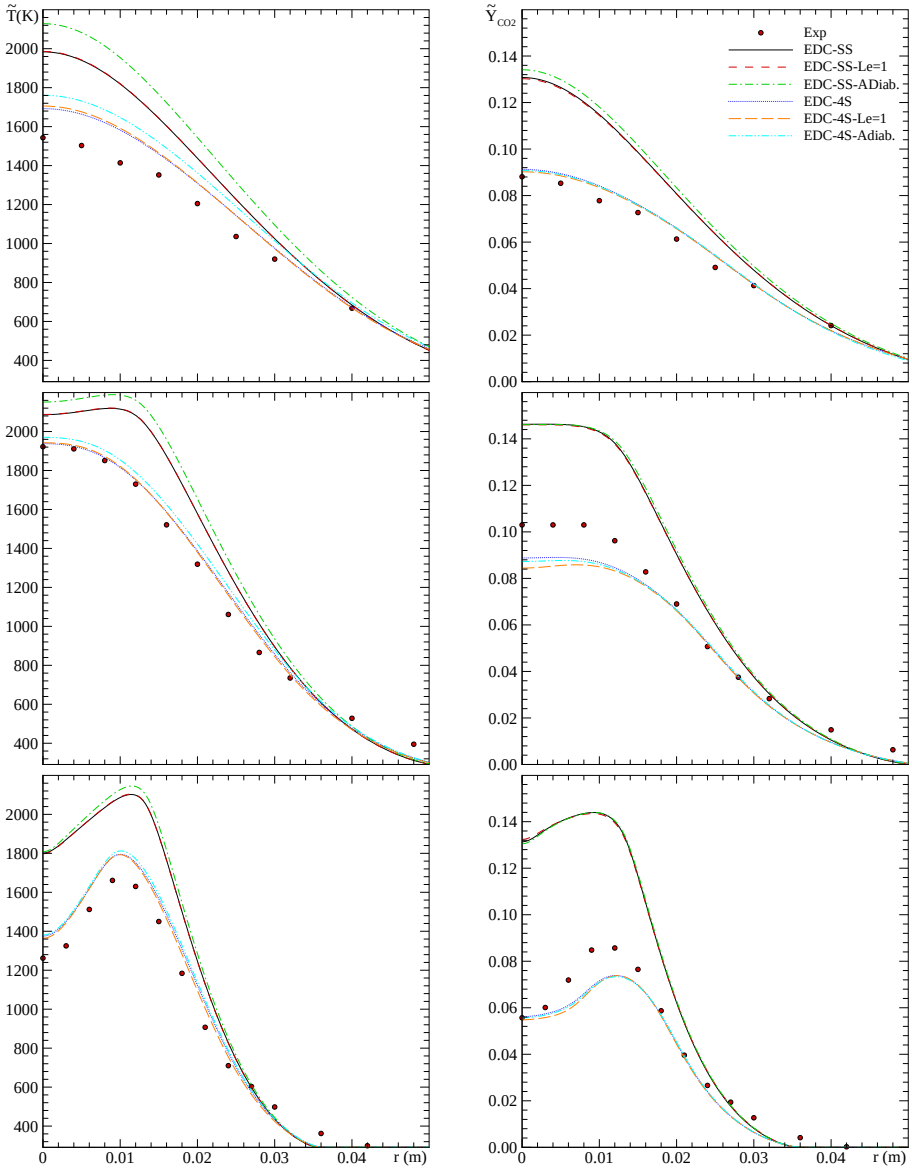

Figure 4.7: Radial profiles for the turbulent piloted methane/air jet flame (Flame D). Eddy dissipation concept (EDC) simulations: z/d=30, 45 and 60 (left: Temperature; right: CO_2 mass fraction). Experimental results in [8].

and as the flame front is achieved, the temperature is increasingly over-predicted by the SF. The peak temperature is about 100 K over-predicted compared to the experimental data. This over-prediction is maintained until the end of the computational domain (outlet). In the radial profiles, SF profiles acquire a clear discrepancy with the experimental data for the flame heights of z/d=30, 45 and 60. This disagreement is attributed to the adiabatic conditions imposed to the steady flamelet simulations.

Major species such as H_2O and CO_2 are properly predicted for the steady flamelet approach. This behaviour is shown for both axial and radial profiles, at each flame height. Even though the over-prediction of temperature, these major species are not significantly affected. On the other hand, radicals such as H_2 and OH are affected for the temperature over-prediction exhibiting also an over-prediction of its production. This effect is larger for H_2 mass fraction. Being the pollutant formation a slow process, it is not properly predicted by the steady flamelet approach. A clear over-prediction of both CO and NO is produced. In figure 4.9d this effect is clearly exposed for the NO production observing the mass fraction profile along the centerline. The peak is more than four times over-predicted. Radial profiles also confirm this behaviour. Even though, radial profiles also show that this disagreement is more important in the post-flame region (see Fig. 4.15). The destruction of NO is not intense enough in this region.

Unsteady flamelet (UF) simulations considering radiation and differential diffusion exhibit an accurate performance to describe the thermal field and the results are well approximated to experimental data. Axial temperature profiles shown in Fig. 4.8 and radial profiles shown in Figs. 4.10 and 4.11 confirm this efficient behaviour. Temperature is specially properly predicted at z/d=3, 7.5 and 60. Otherwise, close to the flame front, temperature is slightly over-predicted (see z/d=30 and 45). In the post-flame region temperature is very similar to experimental data (see z/d=60).

Major species such as H_2O and CO_2 are correctly predicted by UF. Also, production and the posterior destruction of radicals such as H_2 and OH are well described. Pollutant formation (NO and CO mass fractions) is relatively well predicted by unsteady flamelets extensively improving the results obtained with steady flamelets. This improvement is more evident in the post-flame region for both pollutants. Even though, an over-prediction of NO mass fraction is found for the axial and all the radial positions analysed (Figs. 4.9, 4.14 and 4.15). Close to the nozzle (for a flame height of z/d=3 and 7.5), NO mass fraction is dramatically over-predicted for all UF and SF models. Even though these differences are large, the possible errors of experimental data measurements at this zone should be carefully considered. Results obtained in the present study using unsteady flamelets models are in concordance with the results published by Coelho and Peters in [48] using the Eulerian particle flamelet model applied to the same flame configuration.

Simulations considering and neglecting differential diffusion effects are taken into

account with unsteady flamelets simulations. The effect of a non-unity-Lewis number for each species is expected to be unimportant taking into account the results obtained for the EDC model and also the numerical results published in [47, 49, 50]. Time-averaged molecular diffusion terms are small compared to the turbulent scalar flux. Temperature at post-flame regions (see Fig. 4.11 at flame height of z/d=30, 45 and, specially, 60) are better predicted for unsteady flamelets when differential diffusion is neglected. This tendency is also revealed by CO_2 and OH at z/d=45. Even though, the radial profiles of H_2 close to the nozzle (Fig. 4.12) at flame heights of z/d=3, 7.5 and 15, show that differential diffusion has a slightly importance to describe this species mass fraction. This effect is specially seen for z/d=3. As the flame height increase this effect becomes less important. This result confirms the conclusion published by Pitsch in [47].

In the previous chapter, the difficulty to include differential diffusion in flamelet modelling simulations has been shown and highlighted. Given the inherent difficulty to include differential diffusion in the flamelet model simulations and considering that for turbulent flow regimes this effect is not important, the use of a unity-Lewis number for each species ($Le = 1$) is recommended. Some authors suggest the possibility to include differential diffusion only close to the nozzle since this effect appear mainly there and vanish for high Reynolds numbers [47].

On the other hand, unsteady flamelets exhibit and effective capability to predict radiation heat transfer with the optically thin approximation. Adiabatic flame conditions in the flamelet formulation are also considered taken into account both the inclusion or neglection of differential diffusion. Then, each effect can be separately analysed or coupled. A comparison of the same conditions for steady and unsteady flamelets (Adiab. and $Le = 1$) is used to explore the influence of the unsteady term in the flamelet equations. In this conditions, SF and UF show a very similar thermal field and also a similar behaviour of the major species distribution. The main differences arises for species involved in slow processes such as CO and NO. Therefore, the importance to retained the unsteady term in the flamelet equation is shown in the pollutant formation.

4.8.3 Round-jet anomaly effect. The $c_{\epsilon 2}$ turbulence model constant

Given the simple flow configuration of the turbulent flame studied in the present chapter, without any wall that confines the flame or solid elements that could induce recirculating vortices, the turbulent model used in all the simulations is the one proposed in section 4.6.2. The only model constant susceptible to be studied is the modification of $c_{\epsilon 2}$ in order to take into account the round-jet anomaly described in the literature [19] and giving an idea of its influence. Results discussion is supported

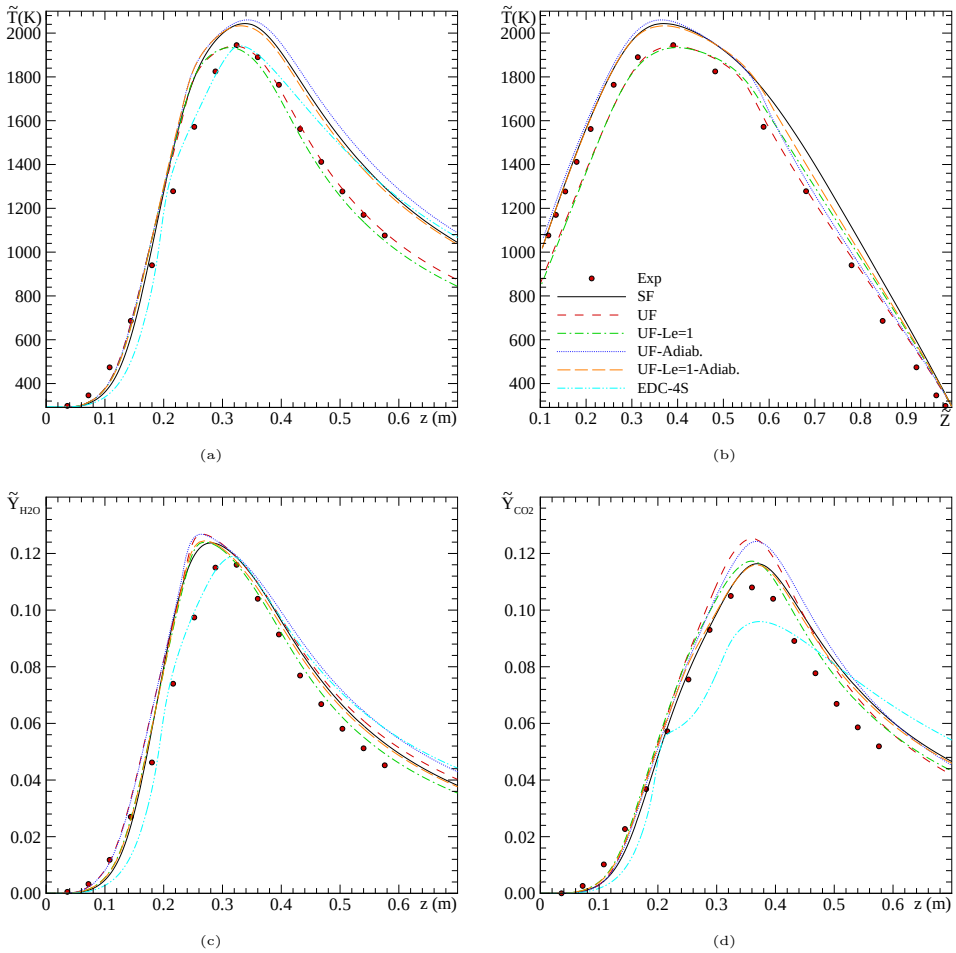

Figure 4.8: Centerline profiles for the turbulent piloted methane/air jet flame (Flame D): (a) Centerline temperature; (b) Centerline temperature conditioned to the mixture fraction; (c) Centerline H_2O mass fraction; (d) Centerline CO_2 mass fraction. Experimental results in [8].

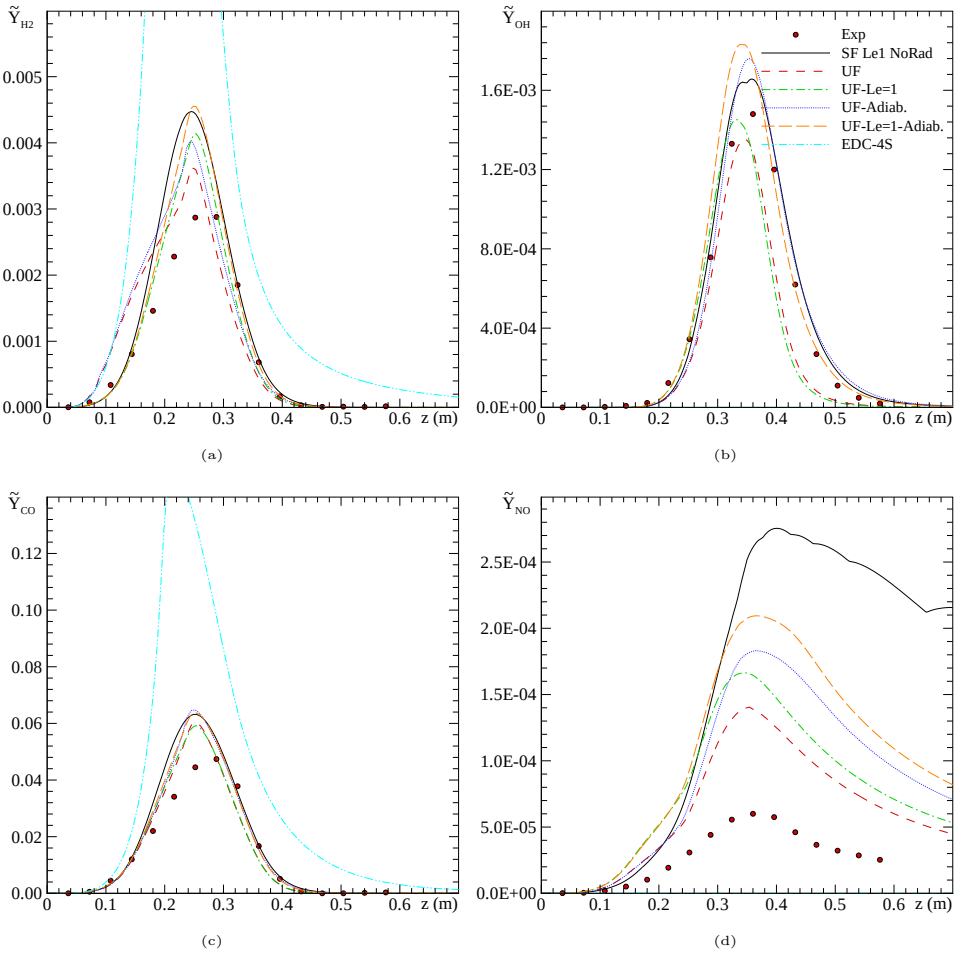

Figure 4.9: Centerline profiles for the turbulent piloted methane/air jet flame (Flame D): (a) Centerline H_2 mass fraction; (b) Centerline OH mass fraction; (c) Centerline CO mass fraction; (d) Centerline NO mass fraction. Experimental results in [8].

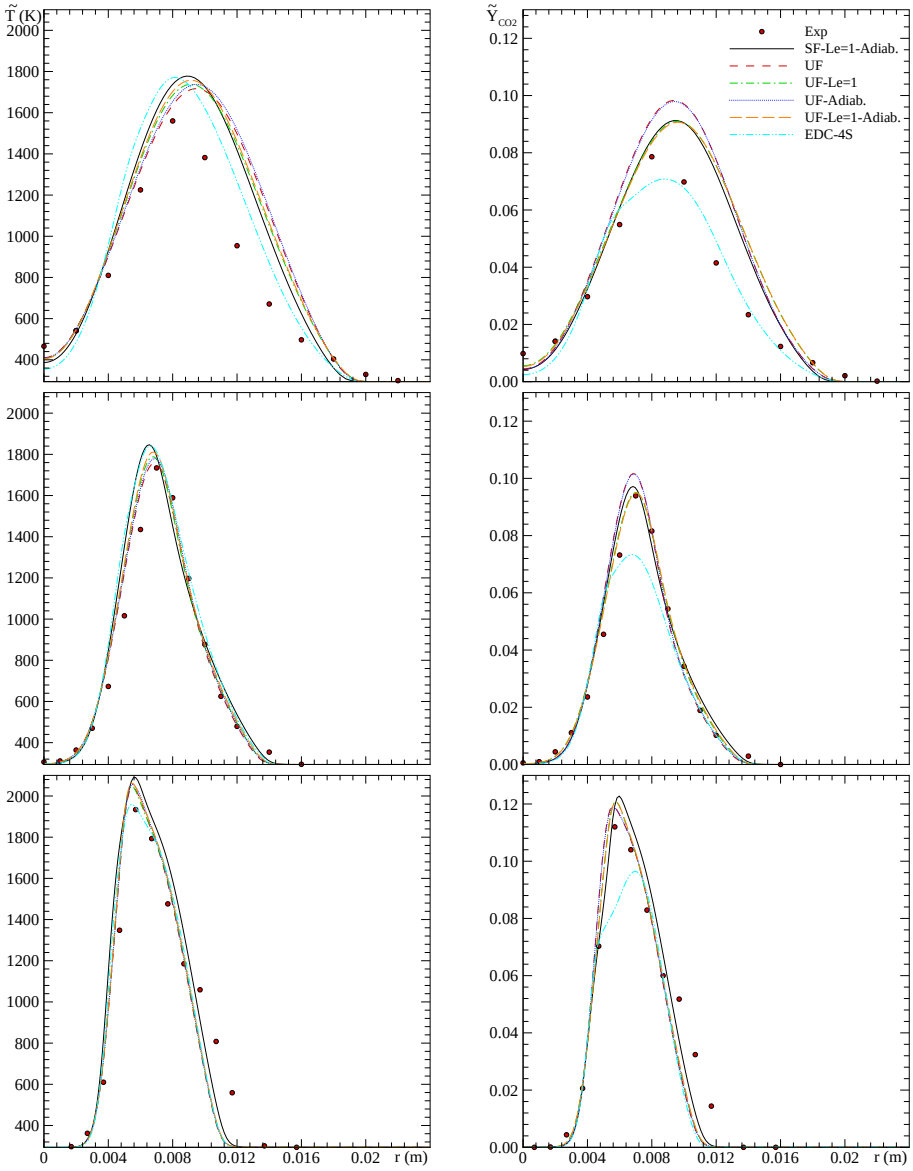

Figure 4.10: Radial profiles for the turbulent piloted methane/air jet flame (Flame D): z/d=3, 7.5 and 15 (left: Temperature; right: CO_2 mass fraction). Experimental results in [8].

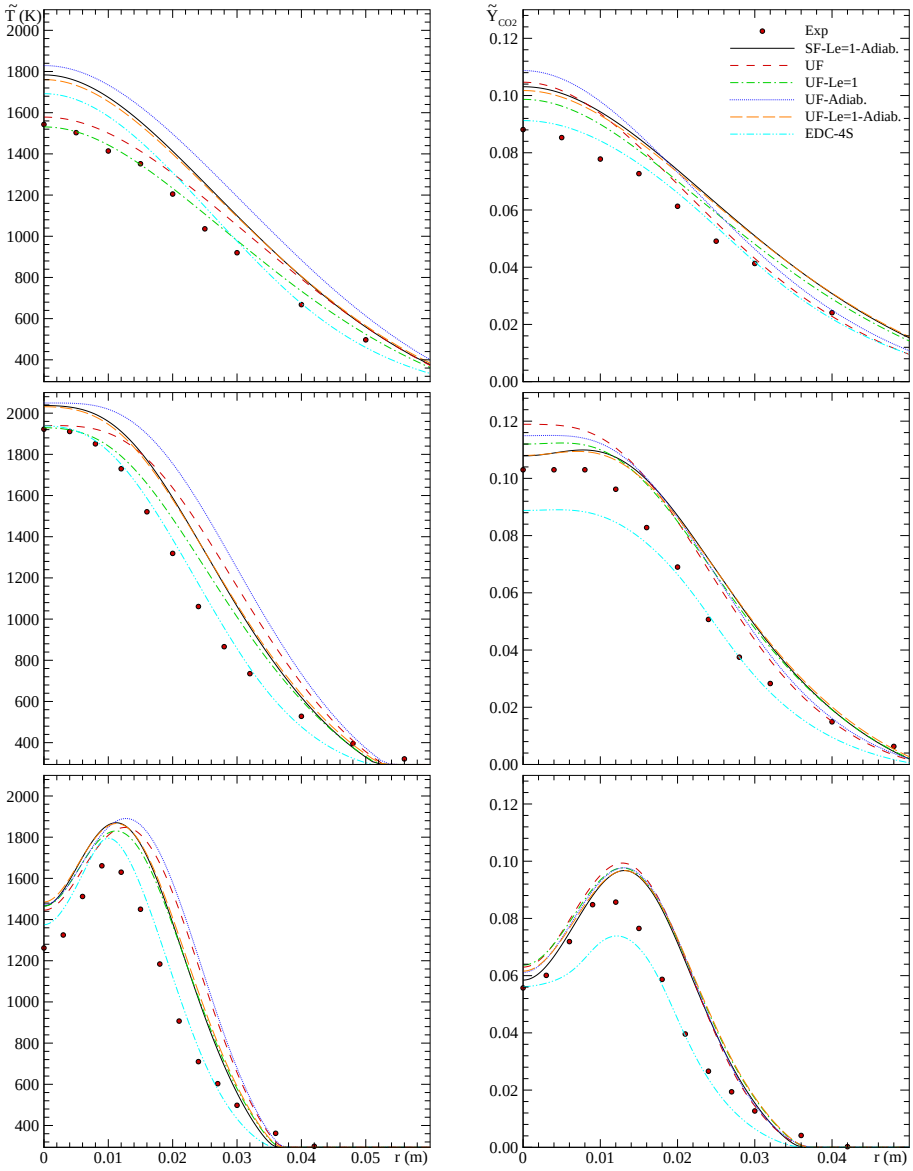

Figure 4.11: Radial profiles for the turbulent piloted methane/air jet flame (Flame D): z/d=30, 45 and 60 (left: Temperature; right: CO_2 mass fraction). Experimental results in [8].

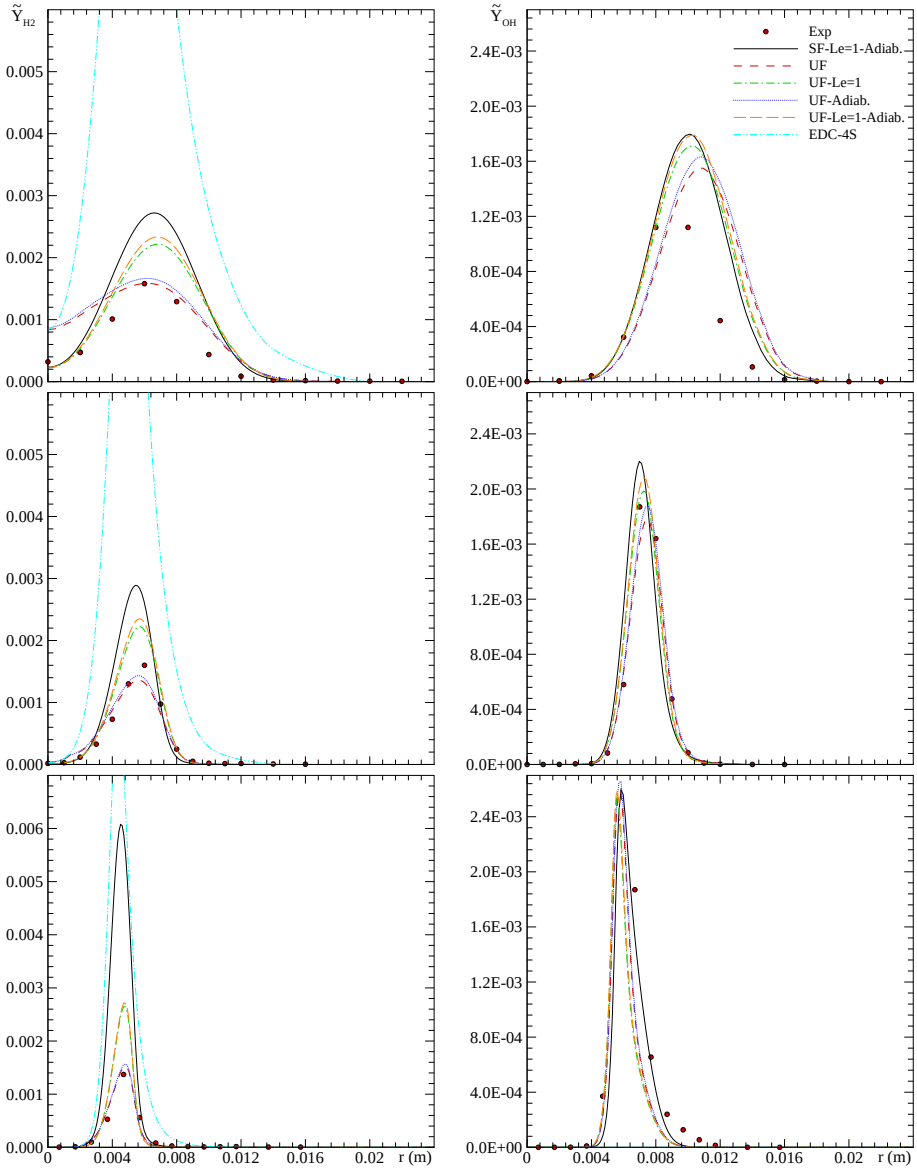

Figure 4.12: Radial profiles for the turbulent piloted methane/air jet flame (Flame D): z/d=3, 7.5 and 15 (left: H_2 mass fraction; right: OH mass fraction). Experimental results in [8].

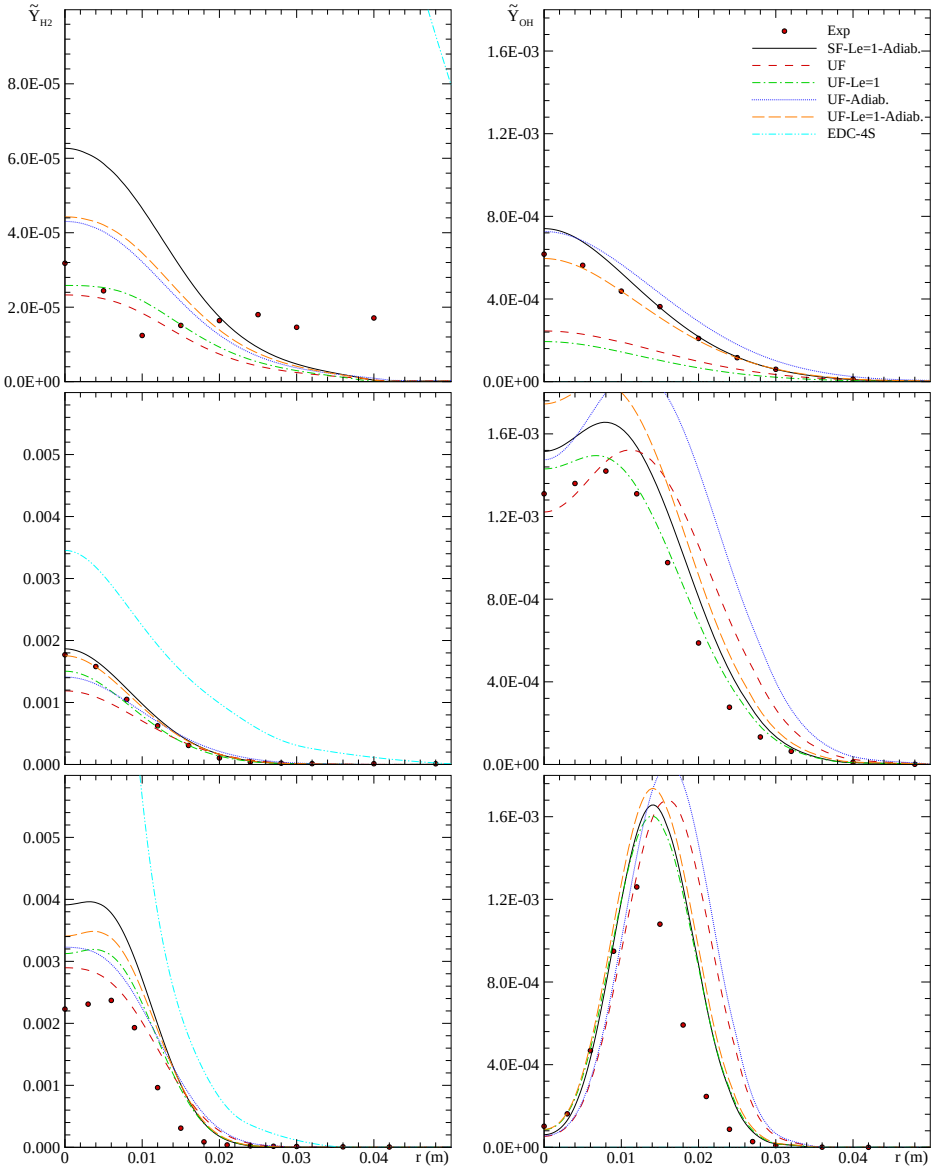

Figure 4.13: Radial profiles for the turbulent piloted methane/air jet flame (Flame D): z/d=30, 45 and 60 (left: H_2 mass fraction; right: OH mass fraction). Experimental results in [8].

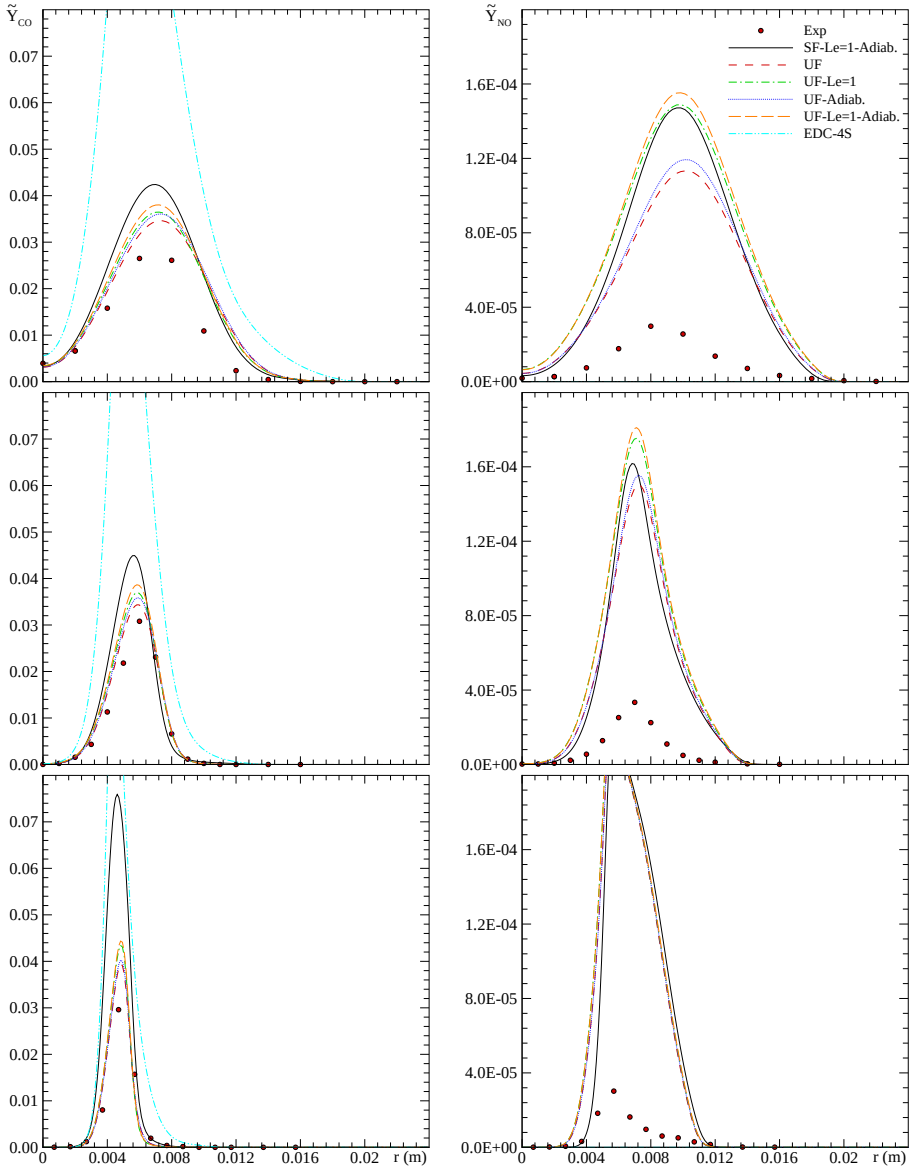

Figure 4.14: Radial profiles for the turbulent piloted methane/air jet flame (Flame D):z/d=3, 7.5 and 15 (left: CO mass fraction; right: NO mass fraction). Experimental results in [8].

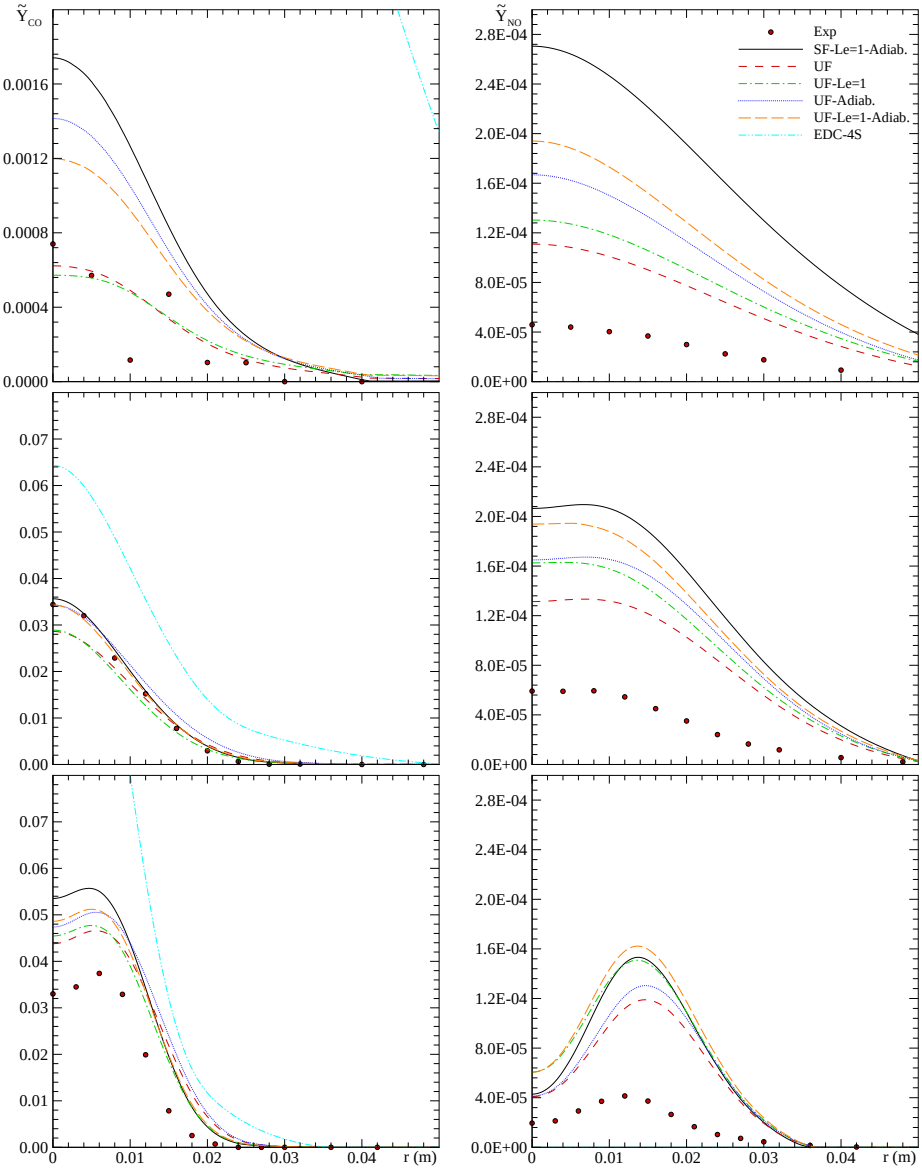

Figure 4.15: Radial profiles for the turbulent piloted methane/air jet flame (Flame D): z/d=30, 45 and 60 (left: CO mass fraction; right: NO mass fraction). Experimental results in [8].

by figure 4.16.

In order to obtain accurate calculations of round jets a modification of the standard model constant $c_{\epsilon 2}$ present in the modelization of the dissipation term of $\widetilde{\epsilon}$ equation (Eq. 4.22) is studied. The standard value is $c_{\epsilon 2}$=1.92 [17]. Different authors, specially in the framework of the *International Workshop on Measurement and Computation of Turbulent Non-premixed Flames* (TNF) [8], recommend a reduction of the constant, say $c_{\epsilon 2}$=1.8. This last value has been employed in all the simulation presented above. In the present section, the influence of this modification is highlighted.

Figure 4.16 shows steady and unsteady flamelet approaches as well as an EDC model simulation with the four-step mechanism (4S) using both turbulent constant possibilities. For the three models, the effect of the modification of the constant is remarkable. Centerline profiles for temperature and for mass fraction of a major species such as CO_2 are plotted and an under-prediction of the flame height is clearly observed when the standard $c_{\epsilon 2}$ is used. This trend is similar for the three models. For unsteady flamelets here presented, the under-prediction of the flame height is about 8 cm while for the steady flamelet simulation is about 9 cm. EDC model has a very similar behaviour. An analogous performance is observed for the CO_2 mass fraction along the centerline.

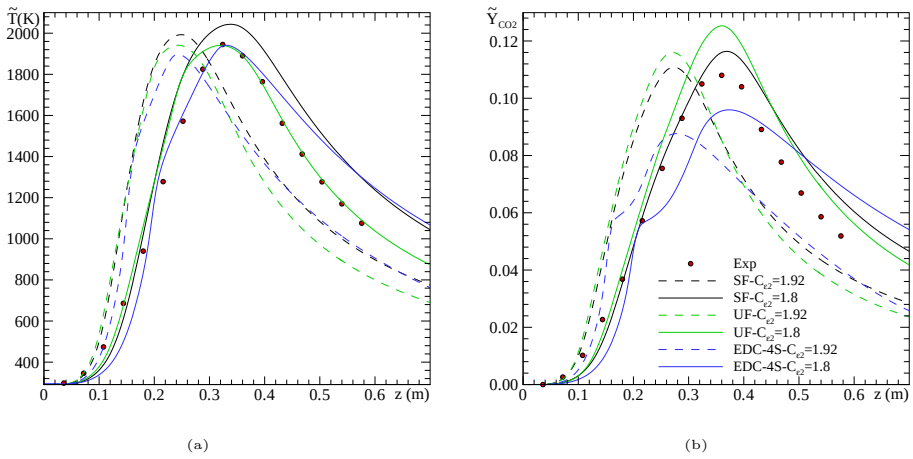

Figure 4.16: Centerline profiles for the turbulent piloted methane/air jet flame (Flame D) comparing the $c_{\epsilon 2}$ turbulent model constant: (a) Temperature; (b) CO_2 mass fraction. Experimental results in [8].

The large impact found in all the cases with the modification of the turbulent model constant $c_{\epsilon 2}$ suggests a deeper study in this direction. Other purposed changes

published in the literature such as the so-called Pope correction [19] are susceptible to be analysed. This study is beyond the scope of the present thesis.

4.9 Conclusions

A brief description of turbulence is exposed in the beginning of this chapter, characterising the turbulence phenomena and its interaction with the chemistry involved in turbulent non-premixed flames. The Favre-averaged governing equations (mass, momentum, energy and species) are presented and the terms in these equations that require a closure are highlighted. A modelization for each term is proposed. Reynolds stresses and scalar turbulent fluxes are modelled by means of eddy-viscosity two-equation models. For the selected test flame, an in order to take into account the round-jet anomaly, the standard $\widetilde{k}-\widetilde{\epsilon}$ model is used in all the simulations with a modification of the model constant for the dissipation term in the $\widetilde{\epsilon}$ equation. Molecular diffusion terms are modelled simply substituting the instantaneous variable by their Favre-averaged value. Radiation heat transfer is approximated by an optically thin model also substituting the instantaneous temperature and mass fraction of the species involved (CO_2, H_2O, CH_4 and CO) by their Favre-averaged. An extended version of the Eddy Dissipation Concept (EDC) to model the time-averaged net production rate present in species equations is introduced. The EDC considered determines the averaged production rate comparing the slowest between the mixing process (characterised by the turbulent mixing time) and the kinetically controlled process by means of the Arrhenius rates.

The laminar flamelet concept (exposed in Chapter 3 and applied for the multidimensional simulation of non-premixed laminar flames) is extended to non-premixed turbulent combustion. Favre-averaged governing equations of the mixture fraction and its variance are formulated. The turbulent scalar fluxes are also modelled by means of the eddy-viscosity two-equation model. The scalar dissipation rate of the fluctuations of the mixture fraction field is related to an average of the scalar dissipation rate described in the previous chapter. This term is modelled considering the turbulent mixing time. Favre-averaged temperature and species mass fraction are obtained integrating the flamelet libraries described in Chapter 3 assuming a β pdf.

The laminar flamelet concept is applied to a piloted non-premixed methane/air turbulent flame, the so-called Flame D by Barlow and Frank [9]. Verified numerical results obtained with steady and unsteady flamelets are compared paying special attention to the prediction of pollutant formation. Unsteady flamelets are capable to reproduce slow processes such as radiation and pollutant formation (CO and NO_x), and therefore, a clear improvement is shown when the transient term in the flamelet equations is retained. The Eddy Dissipation Concept model is also considered with an irreversible single-step reaction mechanism as well as with a reduced mechanism (four-

step). The solutions obtained are considered as illustrative results of the performance of simpler and widely used models applied in industry.

The numerical results obtained for this turbulent flame confirm that the averaged molecular diffusion terms that appear in the governing equations are negligible compared to the turbulent fluxes. This conclusion can be deduced for both EDC and flamelet modelling simulations. On the other hand, and as it was expected, radiation heat transfer is revealed as a key aspect to properly define the thermal level and, consequently, the temperature-dependent species such as NO_x.

The modification introduced in the dissipation term of the $\widetilde{\epsilon}$ equation, the $c_{\epsilon 2}$ constant, to deal with the so-called round-jet anomaly is examined in the last section of this chapter. The results show that this term has a strong influence on the prediction of the flame height.

References

[1] N. Peters. *Turbulent combustion*. Cambridge University Press, 2000.

[2] J. Warnatz, U. Maas, and Dibble R.W. *Combustion*. Springer-Berlag, 1996.

[3] S.B. Pope. *Turbulent Flows*. Cambridge University Press, 2000.

[4] P. Sagaut and M. Germano. *Large Eddy Simulation for Incompressible Flows*. Springer-Berlag, 2001.

[5] D.C. Wilcox. *Turbulence modeling for CFD*. DCW Industries, Inc. CA, 1993.

[6] J.E. Jaramillo, K. Claramunt, C.D. Pérez-Segarra, R. Cònsul, and J. Cadafalch. Numerical study of different RANS models applied to turbulent forced convection. In *Proceedings of the IV International Symposium on Turbulence, Heat and Mass Transfer*, pages 671–680, 2003.

[7] B.F. Magnussen and B.H. Mjertager. Effects on Turbulence on Species Mass Fractions in Methane/Air Jet Flames. In *Proceedings of the Sixteenth Symposium (International) on Combustion*, pages 719–727, 1976.

[8] TNF Workshop, http://www.ca.sandia.gov/TNF.

[9] R.S. Barlow and J.H. Frank. Effects on Turbulence on Species Mass Fractions in Methane/Air Jet Flames. In *Proceedings of the Twenty-Seventh Symposium (International) on Combustion*, pages 1087–1095, 1998.

[10] H. Tennekes and J.L. Lumley. *A first course in turbulence*. The MIT Press, 1972.

[11] J. Cadafalch. *Numerical simulation of turbulent flows. multiblock techniques. verification and experimental validation.* PhD thesis, Universitat Politècnica de Catalunya, 2002.

[12] T. Poinsot and D. Veynante. *Theoretical and Numerical Combustion.* R.T. Edwards, Inc., 2001.

[13] M. Herrmann. *Numerical Simulation of Premixed Turbulent Combustion Based on a Level Set Flamelet Model.* PhD thesis, Universitat Politècnica de Catalunya, 2001.

[14] S.B. Pope. PDF methods for turbulent reactive flows. *Progress in Energy and Combustion Science*, 11:119–192, 1985.

[15] C.D. Pérez-Segarra, A. Oliva, M. Costa, and F. Escanes. Numerical experiments in turbulent natural and mixed convection in internal flows. *International Journal for Numerical Methods for Heat and Fluid Flow*, 5(1):13–33, 1995.

[16] W.P. Jones and B.E. Launder. The prediction of laminarization with a two-equation model of turbulence. *International Journal of Heat and Mass Transfer*, 15:301–314, 1972.

[17] B.E. Launder and B.I. Sharma. Application of the energy dissipation model of turbulence to the calculation of flow near a spinning disc. *Letters in Heat Transfer*, 1:131–138, 1974.

[18] N.Z. Ince and B.E. Launder. Computation of turbulent natural convection in closed rectangular cavities. In *Proceedings of the 2nd U.K. Natural Conference Heat Transfer*, volume 2, pages 1389–1400, 1988.

[19] S.B. Pope. An Explanation of the Turbulent Round-Jet/Plane-Jet Anomaly. *AIAA Journal*, 16:279–281, 1978.

[20] P.J. Coelho, O.J. Teerling, and D. Roekaerts. Spectral radiative effects and turbulence/radiation interaction in a non-luminous turbulent jet diffusion flame. *Combustion and Flame*, 133:75–91, 2003.

[21] X. Zhou, Z. Sun, G. Brenner, and F. Durst. Combustion modeling of turbulent jet diffusion H_2/air flame with detailed chemistry. *International Journal of Heat and Mass Transfer*, 43:2075–2088, 2000.

[22] D.B. Spalding. Mixing and chemical reaction in steady confined turbulent flames. In *Proceedings of the Thirteenth Symposium (International) on Combustion*, pages 649–657, 1971.

[23] X.S. Bai and L. Fuchs. Sensitivity Study of Turbulent Reacting Flow Modeling in Gas Turbine Combustors. *AIAA Journal*, 33(10):1857–1864, 1995.

[24] A. Brink, C. Mueller, P. Kilpinen, and M. Hupa. Possibilities and Limitations of the Eddy Break-Up Model. *Combustion and Flame*, 123:275–279, 2000.

[25] D. Chakraborty, P.J. Paul, and H.S. Mukunda. Evaluation of Combustion Models for High Speed H_2/Air Confined Mixing Layer Using DNS Data. *Combustion and Flame*, 121:195–209, 2000.

[26] H.C. Magel, R. Schneider, B. Risio, U. Schnell, and K.R.G. Hein. Numerical simulation of utility boilers with advanced combustion technologies. In *Proceedings of the Eight International Symposium on Transport Phenomena in Combustion*, 1995.

[27] P.A. Libby and F.A. Williams (ed.). *Turbulent Reacting Flows*. Academic Press, 1994.

[28] D. Veynante and L. Vervisch. Turbulent Combustion Modeling. *Progress in Energy and Combustion Science*, 28:193–266, 2002.

[29] N. Peters. Laminar diffusion flamelet models in non-premixed turbulent combustion. *Progress in Energy and Combustion Science*, 10:319–339, 1984.

[30] J.S. Kim and F.A. Williams. Structures of flow and mixture-fraction fields for counterflow diffusion flames with small stoichiometric mixture fractions. *Journal of Computational Physics*, 53:1551–1566, 1993.

[31] R. Cònsul, C.D. Pérez-Segarra, K. Claramunt, J. Cadafalch, and A. Oliva. Detailed numerical simulation of laminar flames by a parallel multiblock algorithm using loosely coupled computers. *Combustion Theory and Modelling*, 7(3):525–544, 2003.

[32] K. Claramunt, R. Còsul, C.D. Pérez-Segarra, and A. Oliva. Multidimensional mathematical modeling and numerical investigation of co-flow partially premixed methane/air laminar flames. *Combustion and Flame*, 137:444–457, 2004.

[33] J. Cadafalch, C.D. Pérez-Segarra, R. Còsul, and A. Oliva. Verification of finite volume computations on steady state fluid flow and heat transfer. *Journal of Fluids Engineering*, 124:11–21, 2002.

[34] G.P. Smith, D.M. Golden, M. Frenklach, N.W. Moriarty, B. Eiteneer, M. Goldenberg, C.T. Bowman, R.K. Hanson, S. Song, W.C. Gardiner, V.V. Lissianski, and Z. Qin. Gri-Mech 3.0, http://www.me.berkeley.edu/gri_mech/.

[35] H.C. Lange and L.P.H. De Goey. Two-dimensional methane/air flames. *Combustion Science and Technology*, 92:423–427, 1993.

[36] W.P. Jones and R.P. Lindstedt. Global reaction schemes for hydrocarbon combustion. *Combustion and Flame*, 73:233–249, 1988.

[37] R.S. Barlow, A.N. Karpetis, and J.Y. Frank, J.H. Chen. Scalar profiles and NO formation in laminar opposed-flow partially premixed methane/air flames. *Combustion and Flame*, 127:2102–2118, 2001.

[38] S. Mazumder and M.F. Modest. Advanced nongray radiation model coupled with a CFD code for large-scale fire and combustion applications. Technical report, National Sciencie Foundation, 2001.

[39] S.R. Marthur and J.Y. Murthy. Pressure boundary conditions for incompressible flow using unstructured meshes. *Numerical Heat Transfer, Part B*, 32:283–298, 1997.

[40] S.V. Patankar. *Numerical heat transfer and fluid flow.* Hemiosphere Publishing Corporation, 1980.

[41] B.R. Hutchinson and G.D.Raithby. A multigrid method based on the additive correction strategy. *Numerical Heat Transfer, Part B*, 9:511–537, 1986.

[42] J. Cadafalch, A. Oliva, C.D. Pérez-Segarra, M. Costa, and J. Salom. Comparative study of conservative and nonconservative interpolation schemes for the domain decomposition method on laminar incompressible flows. *Numerical Heat Transfer, Part B*, 35(1):65–84, 1999.

[43] R. Cònsul, C.D. Pérez-Segarra, J. Cadafalch, M. Soria, and A. Oliva. Numerical analysis of laminar flames using the domain decomposition method. In *Proceedings of the Fourth European Computational Fluid Dynamics Conference (ECCOMAS CFD)*, volume 1.2, pages 996–1001, 1998.

[44] F. Liu, H. Guo, G.J. Smallwood, O.L. Gülder, and M.D. Matovic. A robust and accurate algorithm of the β-pdf integration and its application to turbulent methane-air diffusion combustion in a gas turbine combustor simulator. *International Journal of Thermal Sciences*, 41:763–772, 2002.

[45] M. Galassi, J. Davies, J. Theiler, B. Gough, G. Jungman, M. Booth, and F. Rossi. GNU Scientific Library Reference Manual (2nd Ed.), ISBN 0954161734, 2003.

[46] H. Pitsch, M. Chen, and N. Peters. Unsteady flamelet modeling of turbulent hydrogen-air diffusion flames. In *Proceedings of the Twenty-Seventh Symposium (International) on Combustion*, pages 1057–1064, 1998.

[47] H. Pitsch. Unsteady flamelet modeling of differential diffusion in turbulent jet diffusion flames. *Combustion and Flame*, 123:358–374, 2000.

[48] P.J. Coelho and N. Peters. Unsteady modelling of a piloted Methane/air jet flame based on the Eulerian particle flamelet model. *Combustion and Flame*, 124:444–465, 2001.

[49] H. Pitsch and H. Steiner. Large-Eddy Simulation of a turbulent piloted methane/air diffusion flame (Sandia Flame D). *Physics of Fluids*, 12(10):2541–2554, 2000.

[50] H. Pitsch, E. Riesmeier, and N. Peters. Unsteady flamelet modeling of Soot Formation in turbulent diffusion flames. *Combustion Science and Technology*, 158:389–406, 2000.